



Understanding dopant and defect effect on H₂S sensing performances of graphene: A first-principles study



Yong-Hui Zhang^{a,*}, Li-Feng Han^a, Yuan-Hua Xiao^a, Dian-Zeng Jia^b, Zhan-Hu Guo^c, Feng Li^{a,*}

^a College of Materials and Chemical Engineering, Zhengzhou University of Light Industry, Zhengzhou 450002, PR China

^b Institute of Applied Chemistry, Xinjiang University, Urumqi 830046, PR China

^c Integrated Composites Laboratory, Dan F. Smith Department of Chemical Engineering, Lamar University, Beaumont, TX 77710, USA

ARTICLE INFO

Article history:

Received 20 September 2012

Received in revised form 23 November 2012

Accepted 29 November 2012

Available online 8 January 2013

Keywords:

Graphene

H₂S

Sensor

Electron transport

ABSTRACT

The interaction between hydrogen sulfite (H₂S) and graphene was investigated by density functional theory calculations and nonequilibrium Green's function formalism. The structural and electronic properties of H₂S–graphene systems were studied by tuning the geometries of H₂S molecule toward 2D nanosheets of pristine, defective and doped graphene. It was found that Ca, Co and Fe doped and defective graphene nanosheets show much higher affinities to H₂S molecule in comparison to pristine graphene. The strong interactions between H₂S and graphene nanosheets modified with transition metals can lead to dramatic changes to the electronic and magnetic properties of graphene. The electronic transport behaviors of Fe-doped graphene nanosheets indicate that the chemical sensors constructed with the materials could exhibit much higher sensitivity for detecting H₂S gas, in comparison with that of devices made with pristine graphene. It is possible to design H₂S chemical sensors with highly improved performances, using graphene nanosheets as sensing materials with appropriate metal dopants or defects. In addition, the graphene doped with Si absorbs H₂S molecule through forming Si–S bond, compared to the weak physisorption of H₂S molecule onto pristine and the B, N doped graphene.

© 2012 Elsevier B.V. All rights reserved.

1. Introduction

The successful syntheses of novel two-dimensional (2D) graphene and the experimental observation of Dirac fermions in graphene-based devices have attracted extensive attention of scientists in diverse disciplines of science and technology due to its unique structural, mechanical, and electronic properties [1]. It is a promising candidate for applications such as spintronic devices, gas sensors, light emitting diodes and photovoltaics [2–5]. Because the performances of graphene-based devices are generally determined by the electronic properties of graphene, experimental and theoretical studies have thus been conducted to understand the interactions of the materials with different chemical species for improving its chemical and physical properties [6,7]. The previous researches in this area have focused on the interactions of small gas molecules, such as CO, NO₂ and NH₃ with the pristine graphene in theory [8] and CO₂ sensing using graphene sheet in experiment [9]. After introducing dopants into 2D nanosheets of graphene, the interactions between small molecules and graphene can be highly enhanced [7,10]. Recently, the functionalized graphene (nanorib-

bon) have also been investigated extensively [11,12]. DNA-decorated graphene [6], show improved performances when working as chemical sensors. Multi-layer graphene nanoribbon networks [13] modified with Pd can be used as functional materials to sense or storage hydrogen [14,15]. It has been found that organic electron acceptors [16], donors [17] or even DNA fragments [18], for instance, can induce significant changes in the electronic structure of graphene. Metal dopant [19] and defect [20] can be used to tune graphene's magnetic property. These theoretical studies could give us clear insight into understanding the bio/chemical sensing behaviors of graphene and thus direct us in designing novel microdevices with optimized performances.

H₂S is a malodorous gas that can lead to death when at a concentration higher than 250 ppm [21], and several groups have worked on fabricating microdevices for detecting the toxic molecule. Recently, L. Mai et al. reported electrical transport and H₂S sensing properties of β-AgVO₃ nanowires [22]. Vertically aligned CuO nanowire array and self-assembled In₂O₃ nanoparticles were also used as building blocks to construct H₂S sensors [23]. Our research in this area has concentrated on the design and fabrication of functional materials with controlled structures and their chemical sensors [24,25]. It was found that the surface modification of ZnO nanowires with Pd nanoparticles can highly enhance the performances of H₂S sensors [26]. While the chemical sensors based on carbon nanotubes [27] and graphene [28,29] were also

* Corresponding authors. Address: 5 Dongfeng Road, Zhengzhou 450002, China. Tel./fax: +86 0371 63556510.

E-mail addresses: yonghuizhang05@gmail.com (Y.-H. Zhang), lifeng696@yahoo.com (F. Li).

investigated extensively, to the best of our knowledge, there is no report in literature concerned with the H₂S sensing performances of materials based on graphene so far.

Herein we report a systematic theoretical study of H₂S sensing ability of graphene doped with elements including B, N, Si, Ca, Co, and Fe, or defected with vacancy by removing one C atom from the 2D nanosheet. The interactions between H₂S molecule and graphene have been investigated carefully for understanding the effects of dopants and defects on the electronic properties of graphene. The transport properties of the modified graphene have been further analyzed semi-quantitatively based on the calculations of current versus voltage (*I*–*V*) curves. It was found that the transport properties of graphene can be tailored effectively by introducing dopants and defects into the 2D sheets. Novel H₂S sensors with highly enhanced sensitivity could be designed using modified graphene as sensing materials. The magnetic property of H₂S/Fe-graphene system will also be discussed.

2. Calculation method and model

The density functional theory (DFT) calculations were performed with CASTEP [30] using ultrasoft pseudopotential, plane-wave basis and periodic boundary conditions. The local density approximation (LDA) with CA-PZ functionality and cut-off energy of 240 eV for the plane-wave basis set were used in all relaxation process. The system investigated was composed of a graphene super cell (12.30 × 12.30 × 10.00 Å, 50 atoms) with a single molecule adsorbed at its central region (Fig. 1). The distance between the adjacent graphene layers was kept as 10 Å. The *k*-point was set to 3 × 3 × 1 for the Brillouin zone integration. The structural configurations of the isolated graphene were optimized through fully relaxing the atomic structures. With the same super cell and *k*-point samplings, the configurations of the graphene/molecule systems were optimized through fully relaxing the atomic structures until the remaining forces were smaller than 0.01 eV/Å. The adsorption energy of H₂S on graphene was calculated as:

$$E_{\text{ad}} = E_{(\text{H}_2\text{S}/\text{graphene})} - E_{(\text{graphene})} - E_{(\text{H}_2\text{S})} \quad (1)$$

For the H₂S/doped-graphene system, the adsorption energy was calculated as:

$$E_{\text{ad}} = E_{(\text{H}_2\text{S}/\text{doped-graphene})} - E_{(\text{doped-graphene})} - E_{(\text{H}_2\text{S})} \quad (2)$$

In the above equations, the $E_{(\text{H}_2\text{S}/\text{graphene})}$, $E_{(\text{graphene})}$, $E_{(\text{H}_2\text{S}/\text{doped-graphene})}$, $E_{(\text{doped-graphene})}$ and $E_{(\text{H}_2\text{S})}$ are the total energies of the relaxed

H₂S/graphene adduct, graphene, H₂S/doped-graphene, doped-graphene and the H₂S molecule, respectively.

Our simulation gave a binding energy of –0.11 eV, which is consistent with the previous reports. Furthermore, Test calculations using a larger supercell (14.76 × 14.76 × 12.00 Å, 72 C atoms), a high *k*-point (35 × 35 × 1) for the Brillouin zone integration, a higher cutoff energy (400 eV) or a larger vacuum gap (12 Å) between the graphene sheets were performed for geometry optimizations and electron transport simulations, respectively, which showed less than 4% improvement to the simulation accuracy. Therefore, our calculation method is believed to be accurate. In literature, GGA and LDA are two common methods used in the investigation on nanomaterials. As indicated by the previous theoretical calculations [31,32], GGA methods tend to underestimate the adsorption energies. For example, GGA suggested that almost no interaction between two graphene layers. In contrast, LDA appears to be more appropriate for studying weak interaction systems such as π-stacking among the graphene layers in 3D graphite, and gives binding energies very close to the experimental results [33].

The electron transport calculations were performed using the ATK package [34], which implements DFT-based real-space, non-equilibrium Green's function (NEGF) formalism [35,36]. The mesh cutoff was chosen as 200 Ry to achieve a reasonable balance between the calculation efficiency and accuracy. The current was calculated by the Landauer–Büttiker formula:

$$I = \frac{2e}{h} \int_{\mu_L}^{\mu_R} dE (f_L(E, V) - f_R(E, V)) \cdot T(E, V_b) \quad (3)$$

where $T(E, V_b)$ represents the electronic transport probability, μ_R and μ_L are the chemical potentials of the right and left electrodes, and V_b is the applied bias voltage across the electrodes.

3. Results and discussion

To understand the most favorable binding configuration of H₂S molecule on the pristine graphene, two major possible sites among seven initial adsorption configurations were studied carefully (Fig. 1). One involves the interaction of the H₂S through its sulfur atom, while the other through its two hydrogen atoms. The sulfur end of H₂S could be positioned above a graphene carbon atom, between two bonded graphene carbon atoms, or above the center of a six-membered carbon ring (6MR). The H₂S molecule can also be initially placed with its two hydrogen atoms pointing towards the graphene nanosheet, including above the center of 6MR, cyclo-addition configuration with C–C bond of the graphene. Several

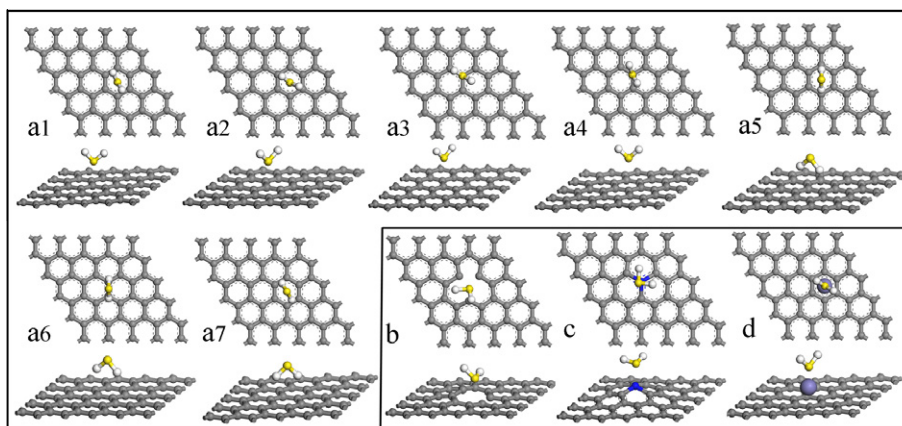


Fig. 1. Top view of the relaxed structures of different adsorption configurations for H₂S/graphene (a1–a7), H₂S/defect-graphene (b), H₂S/Si-graphene (c), and H₂S/metal-graphene (d). C, H, S, Si, and metal atoms are shown in gray, white, yellow, blue, and purple, respectively. (For interpretation of the references to color in this figure legend, the reader is referred to the web version of this article.)

Table 1

Adsorption energy (E_{ad}), equilibrium graphene–molecule distance (d) (defined as the shortest atom-to-atom distance), and Mulliken charge (Q) of small molecule adsorbed on outer surface of graphene.

System	E_{ad} (eV)	d (Å)	Q (e) ^a
a1	−0.13	3.47	0
a2	−0.12	3.38	0
a3	−0.11	3.28	0
a4	−0.11	3.30	0
a5	−0.16	2.64	0.01
a6	−0.15	2.51	0
a7	−0.17	2.58	0
b-defect	−0.91	1.77	0.74
c1-B	−0.11	3.26	0.01
c1-N	−0.14	3.22	0.01
c1-Si	−0.94	2.53	0.26
d1-Ca	−0.66	4.81	0.04
d1-Co	−1.80	3.77	1.16
d1-Fe	−1.92	3.70	1.23

^a Q is defined as the total Mulliken charge on the molecule, and negative number means charge transfer from graphene to molecule.

other configurations with the H₂S molecule placed parallel to the hexagonal plane were also tested. Each structure was fully relaxed, and the calculated adsorption energy, charge transfer, and distance between the adsorbed molecule and the graphene nanosheets are summarized in Table 1. After full relaxation, the configuration with the two hydrogen atoms of adsorbed H₂S pointing to the 2D nanosheets and paralleling to the graphene plane along the axis through the midpoint of two opposite C–C bonds in the 6MR was found to be the most stable one for the pristine graphene (Fig. 1, a7). The adsorption energy (E_{ad}) of this system is −0.17 eV, and the molecule-sheet distance (d) is 2.58 Å. The relatively small E_{ad} and large d values indicate that H₂S molecules undergo weak physisorption on the pristine graphene. The calculated charges of H₂S adsorbed on graphene from Mulliken population analysis are also provided in Table 1. For the most stable configuration (Fig. 1, a7), there is no charge transfer between graphene and H₂S, which also verifies their weak interaction. The results reveal that the pristine graphene is insensitive to H₂S molecule.

For the graphene with defects, the configuration with the plane of H₂S molecule tilting to the graphene nanosheet and the sulfur atom pointing towards the vacancy is found to be the most favorable one (Fig. 1b). The calculation results indicate that the carbon atoms close to the vacancy defect provide stronger binding sites for the H₂S molecule than those further away from the vacancy.

The minimum atom to atom distance between H₂S and the defective graphene is 1.77 Å. This distance is much shorter than that of other types of configurations (Fig. 1, a1–a7), which ranges from 2.58 to 3.57 Å. The adsorption energy of H₂S on the defective graphene can reach −0.91 eV, which is more than five times higher than that of the pristine graphene. The strong interaction should be attributed to the presence of dangling bonds in the defective graphene caused by the missed carbon atom.

The configurations for graphene doped with B and N interacting with H₂S were also studied. When one carbon atom is substituted by B or N atom in the super cell (assigned to B-graphene or N-graphene, respectively), it is found that the geometric structures of the doped graphene nanosheets have a planar configuration before and after adsorption of H₂S molecule [7]. After doping B and N atom into graphene nanosheet, the bond length (l) at the doping site changes from $l_{\text{C-C}} = 1.42$ Å to $l_{\text{C-B}} = 1.48$ Å and $l_{\text{C-N}} = 1.41$ Å, respectively, which agree well with previous theoretical works in B-graphene, N-graphene and doped carbon nanotubes [37,38]. Furthermore, the bond length of doped graphene stays unchanged after adsorbing H₂S. This indicates that the interaction is weak between H₂S molecule and graphene doped with B or N. The adsorption energies for the B-graphene and N-graphene are −0.11 eV and −0.14 eV, respectively, and these results further confirm that they exhibit weaker bindings in comparison with the interaction between H₂S and pristine graphene of −0.17 eV.

In contrast, the geometry of graphene doped with Si (assigned to Si-graphene) as shown in Fig. 1c deforms dramatically before and after adsorbing a H₂S molecule, which is in agreement with previous literatures about Si-doped graphene sensing for small molecules [39,40]. The Si atom is slightly pulled out from the sheet by H₂S molecule, which leads to a significant change in the local geometry of the materials. The three associated C–Si–C angles thus change from 119.99°, 119.99° and 120.0° to 109.33°, 109.38° and 109.09°, respectively. The deviation of C–Si–C bond angles from the standard angle of sp² hybridization of 120° clearly indicates that the Si atom near the adsorption site has changed to a more sp³-like hybridization. Meanwhile, the lengths of three associated C–Si bonds increase from 1.65, 1.65, and 1.65 Å to 1.720, 1.718, and 1.717 Å, respectively. Compared to the distance of around 3.00 Å between the pristine graphene sheet and the S atom of physisorbed H₂S, the sheet-molecule distance between the Si-graphene and H₂S molecule is shorten to 2.53 Å. The results indicate that H₂S molecule is chemisorbed onto the Si-graphene. In addition, the E_{ad} of H₂S on Si-graphene is found to be −0.94 eV, which confirms that the Si-graphene is more favorable for H₂S

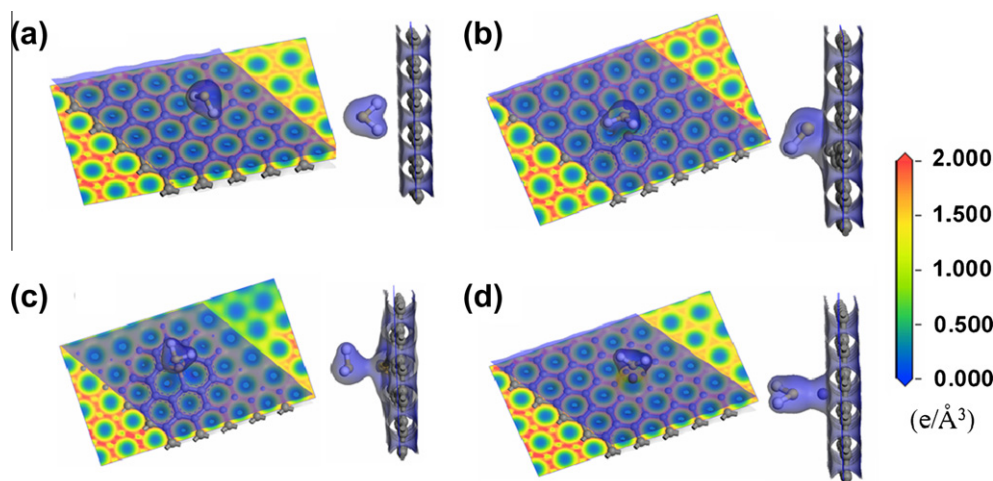


Fig. 2. Electronic total charge densities for (a) H₂S/graphene, (b) H₂S/defect-graphene, (c) H₂S/Si-graphene, and (d) H₂S/Fe-graphene.

adsorption than the pristine graphene. The adsorption energy of H_2S on Si-graphene is comparable to the adsorption energies reported in previous investigations on sensors based on doped CNT, such as NH_3/B -doped CNT (-0.70 eV), NO_2/N -doped CNT (-0.59 eV) and CO/B -doped CNT (-0.85 eV) [41–43]. The results suggest that the Si-graphene is a good sensing material for detecting H_2S , compared to pristine graphene, B-graphene and N-graphene.

In order to enhance the sensing performances of H_2S sensors made with materials based on graphene, we further investigated the adsorption (Table 1) of H_2S molecule on the surface of graphene substituted with transition metal atoms including Ca, Co and Fe. It was found that the three metal-doped graphene can bind H_2S molecule with adsorption energies of -0.66 , -1.80 and -1.92 eV, respectively, which (Co and Fe) are more than one order of magnitude higher than that of the pristine graphene, and are also much higher than that of Si-graphene. The hybrids of transition metal-doped graphene are thus expected to exhibit highly enhanced sensing ability for detecting H_2S molecule, compared to pristine, B-graphene, N-graphene and Si-graphene. Because absorption energy of H_2S molecule on the surface of Fe-graphene is the highest among the metal/graphene, the $\text{H}_2\text{S}/\text{Fe}$ -graphene was thus compared to pristine, defect- and Si-graphene systems for further understanding the electric and magnetic properties of doped graphene. Though the above calculation suggests that the Si-graphene or metal-graphene exhibit improved sensing properties than the pristine graphene, it is worth noting that the strong

binding between the doped graphene and H_2S may imply that the desorption of the H_2S could be difficult, and the devices may suffer from longer recovery time. Possible solutions to this problem could include vacuum annealing [3], UV irradiation [44] or electric field [45] assisted desorption method.

The electronic total charge density plot for the $\text{H}_2\text{S}/\text{pristine}$ graphene is compared with that of the H_2S on the defect-, Si- and Fe-doped graphene in Fig. 2. There is no electron orbital overlap between H_2S molecule and the pristine graphene observed in Fig. 2a. In contrast, Fig. 2b–d shows that all of the three electronic charge plots between H_2S and the defect-, Si- and Fe-doped graphene are strongly overlapped. The results indicate that there are more orbital mixing and larger charge transfer in the three systems, compared to pristine graphene. The total charge density analysis illustrates that only weak physisorption takes place between H_2S molecule and the pristine graphene, in comparison to the strong binding sites of Fe-, defect- and Si-graphene for chemisorption of H_2S . Because the orbital overlap between H_2S and Fe-graphene is much stronger than that between H_2S and pristine, defect and Si-doped graphene, the Fe-graphene system is expected to show significant change in its electronic properties upon H_2S adsorption. It is thus safe for us to conclude that the Fe-graphene system is more suitable for sensing H_2S , compared to the others.

The electron transfer between H_2S and the graphene nanosheets was obtained from the Mulliken population analysis (Table 1), which may be qualitatively understood by the fact that the H_2S adsorption tends to transform the atoms at binding sites from

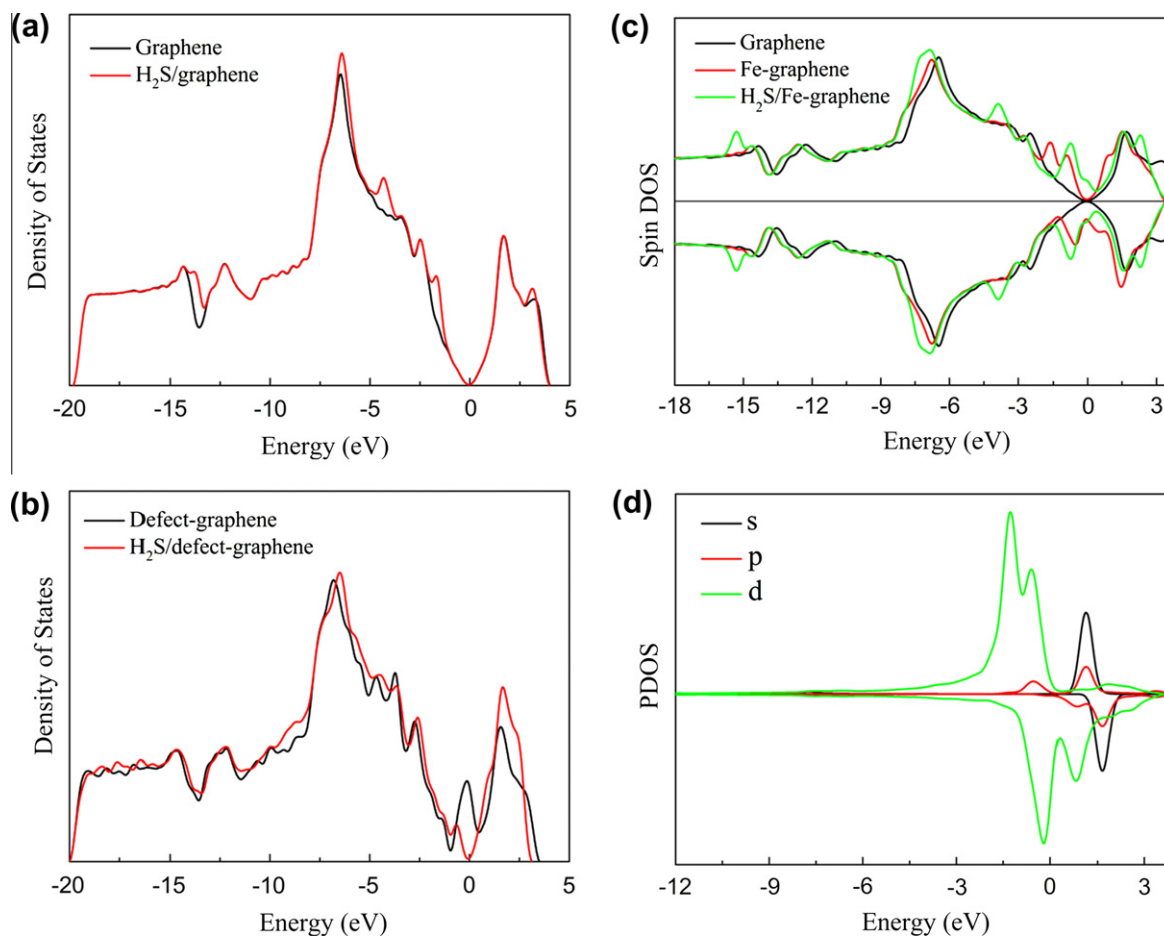


Fig. 3. (a and b) Total electronic density of states for pristine and defect-graphene (black curves) and molecule-graphene systems (red curves) calculated for the corresponding configurations shown in Fig. 1a7 and b. (c) The spin total electronic density of states for pristine, Fe-graphene, and $\text{H}_2\text{S}/\text{Fe}$ -graphene. (d) The PDOS of Fe in Fe-graphene. The Fermi level is set to zero. (For interpretation of the references to color in this figure legend, the reader is referred to the web version of this article.)

sp^2 hybridization to more sp^3 -like hybridization. It was found that a large charge transfer (1.23 |e|) from H_2S to graphene occurs in the presence of Fe atom, and it also takes place in those systems from H_2S to defect-graphene (0.74 |e|) and Si-graphene (0.26 |e|). The H_2S molecule acts as the electron donor in the adsorption process. The high adsorption energy and large electron density overlap observed in the H_2S/Fe -graphene system indicate the formation of coordination bond between H_2S molecule and Fe atom.

To better understand the change in the electronic structure aroise by H_2S gas adsorption, the electronic densities of states (DOSs) are calculated for the systems of H_2S on pristine, defect- and Fe-graphene. Fig. 3 shows the DOS for the representative systems. The adsorption energies calculated reveal that the interaction between H_2S and the pristine graphene is weak. The DOS structure of H_2S /graphene system as shown in Fig. 3a, which show little change after the adsorption of H_2S molecule, clearly verifies the weak interaction again. The contributions of the H_2S electronic levels to the total DOS for pristine, defect- and Fe-graphene are localized between -7.5 and -1.2 eV in the valence bands and around 2.5 eV in the conduction bands, which are far away from the Fermi level.

In contrast, the DOS of H_2S on defective graphene as shown in Fig. 3b is dramatically changed due to the strong molecule-graphene interactions. Compared to that of pristine graphene, the DOS of defect-graphene exhibits a large peak appearing just above the Fermi level. This peak indicates that the system is strongly metallic and a significant increase in the conductivity of defect-graphene is expected in comparison with the pristine graphene.

After the chemisorption of H_2S molecule, the system becomes more like a semiconductor and exhibits a drop of the DOS near the Fermi level. The DOS analysis also indicates that the interaction between H_2S and the defect-graphene is stronger than that of pristine graphene. The adsorption of H_2S onto the surface of defect-graphene can move the major band features to a higher energy; in other words, the Fermi level of the system shifts towards lower energy. It is consistent with the results based on the analysis of adsorption energy values of the two systems. Such an enhancement in the interaction between H_2S molecule and defect-graphene can be directly associated with the rearrangement of the sheet structure of graphene in the presence of H_2S molecule [46].

Considering the strong magnetic property of Fe atom, both Fe-graphene and H_2S/Fe -graphene could be also magnetic. The spin up channel of the Fe-graphene shows two new states, one near -1.0 eV in the valence band and the other near 1.0 eV in the conduction band (Fig. 3c). The zero-gap semiconducting property of the graphene is maintained in the spin up channel of the Fe-graphene, but the spin down channel shows non-zero density of states around the Fermi level. The results suggest that the Fe-graphene is also half-metallic. It is observed that the interaction between graphene and Fe induces significant shifts between the up and down spin DOSs, which should result in a high magnetic moment. The magnetic moment of the Fe-graphene is calculated to be 2.28 μ_B , which is almost twice the value of the Co-graphene. For the H_2S/Fe -graphene, Fig. 3c shows that both spin up and spin down channels move toward lower energy direction. Interestingly, there is no shift observed in the spin DOSs of the H_2S/Fe -graphene

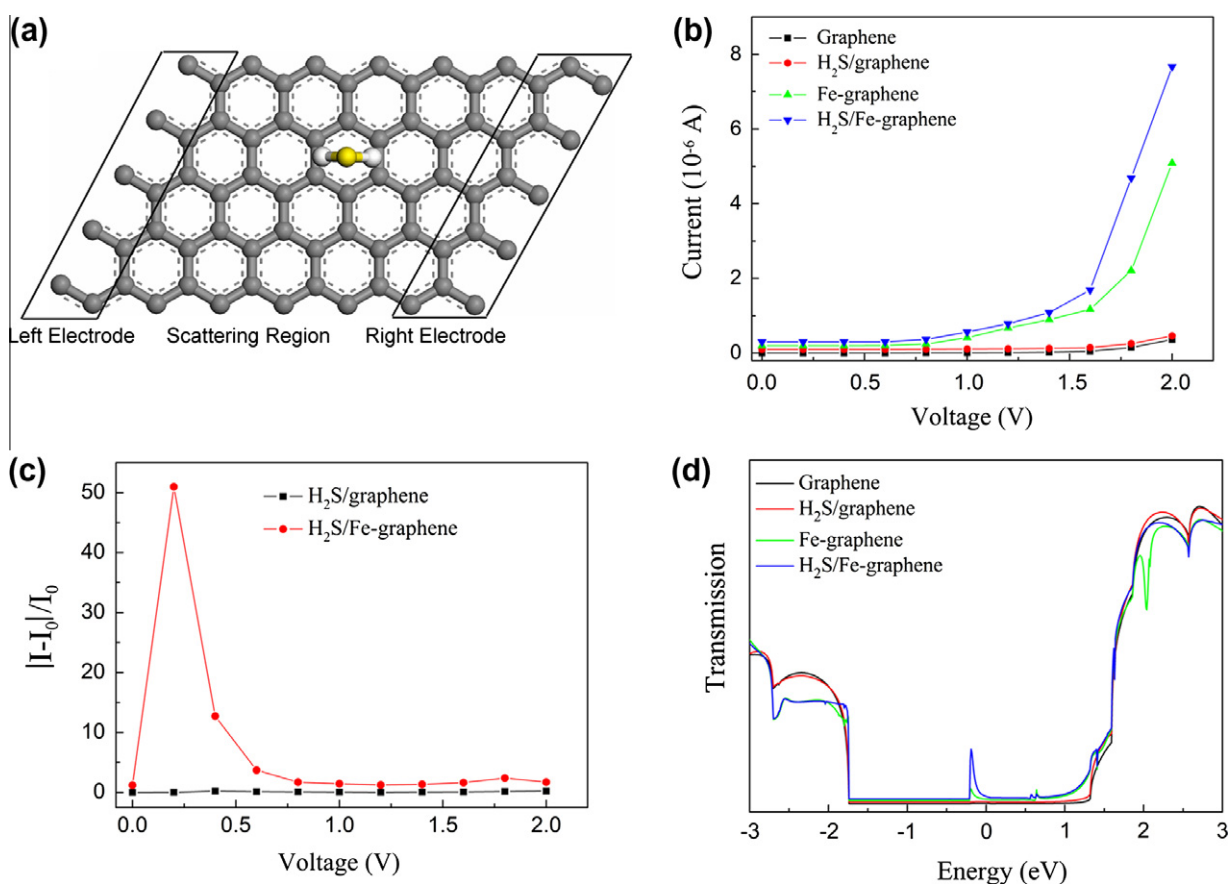


Fig. 4. (a) A schematic illustration of the graphene-based chemical sensor for detecting H_2S gas molecules. (b) The I - V curves of the two electrode devices based on pristine graphene (black), H_2S /graphene (red), Fe-graphene (green) and H_2S/Fe -graphene (blue). (c) The normalized I - V curves of the graphene and Fe-graphene. (d) The transmission of the above junctions under a bias voltage of 1.8 V. It should be noted that the I - V curves are offset 1×10^{-7} A in (b), 1.2 in (c) and 0.02 in (d) from each other for clarity. (For interpretation of the references to color in this figure legend, the reader is referred to the web version of this article.)

system, which indicates that H₂S can turn the magnetic Fe–graphene into nonmagnetic materials. The partial DOSs (PDOSs) of Fe in Fe–graphene are shown in Fig. 3d. The s orbitals of Fe in Fe–graphene contribute to the states near 1.11 eV and 1.62 eV. The p orbitals contribute to the states –0.49 eV below the Fermi level and between 1.10 eV and 1.68 eV above the Fermi level. Meanwhile, the d-orbitals give much stronger intensity, suggesting that the magnetic property mainly comes from the d-orbitals. In the spin-up channel of the Fe–graphene, the d orbitals give two major peaks below the Fermi level, with an energy difference of 0.67 eV, and in the spin-down channel of Fe–graphene, d orbitals split up two energy –0.23 eV and 0.77 eV. The PDOSs are clearly different in the spin-up and spin-down channels, which indicates magnetic moment occurs.

The magnetic properties of H₂S/Fe–graphene system can be explained by the d-orbital splitting of graphene, which could be understood by the classic Ligand Field Theory (LFT) [47–49]. The charge population results indicate that Fe atom bear two positive charges in the H₂S/Fe–graphene complexes, hence it has 6 d-electrons. According to earlier theoretical and experimental work [50], the Spin-Pairing Energy (SPE) of d⁶ transition metal cation is around 1.49 eV. As suggested by the d-band splitting values in the above PDOS calculation, the Δ (Ligand Field Splitting Parameters) values of Fe–graphene system are very small. So, each of the five d-orbitals is occupied by one electron to form “high spin” complexes before any pairing occurs in according to Hund’s rule. In the case of H₂S/Fe–graphene, the system gives a large Δ value of 2.26 eV, which is much higher than the SPE of 1.49 eV. Therefore, the three orbitals with lower energy are completely filled before population of the upper sets start filling in according to the Aufbau principle, so that the 6 d-electrons all exist in paired state, which has resulted in zero magnetic moment.

The *I*–*V* calculation using NEGF method can semi-quantitatively assess the feasibility of using graphene as a sensing material for detecting gas molecules. We further investigated the effects of H₂S molecule adsorption on the transport properties of electrical devices based on graphene (Fig. 4a). The *I*–*V* curve of the pristine graphene exhibits clear non-linear behavior, which is consistent with its zero-gap semiconductor property. The calculated *I*–*V* curves of the pristine graphene and H₂S/graphene systems are very similar (Fig. 4b). In the bias range of 0–3.0 V, the largest current difference between the two systems is less than 2%. This indicates that the response of pristine graphene to H₂S molecule is far from enough for the practical sensing applications. In contrast, the simulated *I*–*V* curves for the pristine graphene and Fe–graphene systems before and after H₂S adsorption are compared in Fig. 4a. The Fe–graphene is much more conductive than the pristine graphene. This may be resulted from the Fe atom donating its 3d electron density into the fact that π orbital of the graphene and the π -states of graphene are hybridized with the 4s and 3d electrons of Fe atom near Fermi level [50]. After normalized against the intrinsic conductivity of the corresponding graphene (Fig. 4c), the sensitivity of Fe–graphene to H₂S is found to be dependent on the bias voltage, and two bias windows of high sensitivity are visible between 0–0.6 V and 1.6–2.0 V, respectively. At the bias voltage of 1.8 V, the Fe–graphene shows a sensitivity of nearly 10 times higher than that of the pristine graphene (Fig. 4c). At the optimum bias voltage of 0.2 V, the Fe–graphene shows a sensitivity of nearly 1900 times higher than that of the pristine graphene. The *I*–*V* results are in accordance with the transmission spectra shown in Fig. 4d. The transmissions of graphene and the H₂S/graphene are close to zero around the Fermi level with poor electron transport channels. In contrast, the Fe–graphene has a peak below the Fermi level whereas the H₂S/Fe–graphene has a high peak above the Fermi level. The Fe–graphene and H₂S/Fe–graphene can provide good electron transport channels and therefore have good conductance.

4. Conclusion

In summary, first-principles calculations reveal that graphene modified with Fe and defect exhibit highly enhanced H₂S sensing behaviors, compared to that of pristine graphene when exposed to gaseous H₂S molecule. Doping graphene with B or N is not a promising route for improving H₂S molecule adsorption. In contrast, H₂S can adsorb on graphene surface strongly when lattice defect or doping Si is introduced into the nanosheet. Metal-doped graphene nanosheets are able to chemically bind H₂S. The changes in the electronic structure produced by absorption and orbital hybridization are confirmed by a large change in conductivity. This makes it possible to use metal-doped graphene as sensing materials for designing novel H₂S sensors.

Acknowledgements

The authors are grateful to the financial support from the National Natural Science Foundation of China (NSFC. 21141005 and 21071130), the School Doctor Foundation of Zhengzhou University of Light Industry (Grant No. 2010BSJJ014), Open Foundation of State Laboratory of Surface & Interface Science and Technology (SLSIST2012001), the Education Department of Henan Province (No. 12B150030), and Outstanding Scholar Program of Henan Province (114200510012).

References

- [1] K.S. Novoselov, A.K. Geim, S.V. Morozov, D. Jiang, Y. Zhang, S.V. Dubonos, I.V. Grigorieva, A.A. Firsov, *Science* 306 (2004) 666.
- [2] S. Stankovich, D.A. Dikin, G.H.B. Dommett, K.M. Kohlhaas, E.J. Zimney, E.A. Stach, R.D. Piner, S.T. Nguyen, R.S. Ruoff, *Nature* 442 (2006) 282.
- [3] F. Schedin, A.K. Geim, S.V. Moezov, E.W. Hill, P. Blake, M.I. Katsnelson, K.S. Novoselov, *Nat. Mater.* 6 (2007) 652.
- [4] I.I. Barbolina, K.S. Novoselov, S.V. Morozov, S.V. Dubonos, M. Missous, A.O. Volkov, D.A. Christian, I.V. Grigorieva, A.K. Geim, *Appl. Phys. Lett.* 88 (2006) 013901.
- [5] C.-A. Di, D. Wei, G. Yu, Y. Liu, Y. Guo, D. Zhu, *Adv. Mater.* 20 (2008) 3289.
- [6] Y. Lu, B.R. Goldsmith, N.J. Kybert, A.T.C. Johnson, *Appl. Phys. Lett.* 97 (2010) 083107.
- [7] Z.M. Ao, J. Yang, S. Li, Q. Jiang, *Chem. Phys. Lett.* 461 (2008) 276.
- [8] O. Leenaerts, B. Partoens, F.M. Peeters, *Phys. Rev. B* 77 (2008) 125416.
- [9] H.J. Yoon, D.H. Jun, J.H. Yang, Z. Zhou, S.S. Yang, M.M.-C. Cheng, *Sens. Actuators, B* 157 (2011) 310.
- [10] Y.-H. Zhang, Y.-B. Chen, K.-G. Zhou, C.-H. Liu, J. Zeng, H.-L. Zhang, Y. Peng, *Nanotechnology* 20 (2009) 185504.
- [11] X.Q. Deng, Z.H. Zhang, G.P. Tang, Z.Q. Fan, M. Qiu, C. Guo, *Appl. Phys. Lett.* 100 (2012) 063107.
- [12] H. Huang, Z. Li, J. She, W. Wang, *J. Appl. Phys.* 111 (2012) 054317.
- [13] J.L. Johnson, A. Behnam, S.J. Pearson, A. Ural, *Adv. Mater.* 22 (2010) 4877.
- [14] D. Li, Y. Ouyang, J. Li, Y. Sun, L. Chen, *Solid State Commun.* 152 (2012) 422.
- [15] J. Li, X. Wang, K. Liu, Y. Sun, L. Chen, *Solid State Commun.* 152 (2012) 386.
- [16] W. Chen, S. Chen, D.C. Qi, X.Y. Gao, A.T.S. Wee, *J. Am. Chem. Soc.* 129 (2007) 10418.
- [17] A.K. Manna, S.K. Pati, *Chem. Asian J.* 4 (2009) 855.
- [18] S. Gowtham, R.H. Scheicher, R. Ahuja, R. Pandey, S.P. Karna, *Phys. Rev. B* 76 (2007) 033401.
- [19] H. Jöhl, J. Wu, S.W. Ong, H.C. Kang, *Phys. Rev. B* 83 (2011) 205408.
- [20] F.M. Hu, J.E. Gubernatis, H.-Q. Lin, Y.-C. Li, R.M. Nieminen, *Phys. Rev. B* 85 (2012) 115442.
- [21] W.H. Tao, C.H. Tsai, *Sens. Actuators, B* 81 (2002) 237.
- [22] L. Mai, L. Xu, Q. Gao, C. Han, B. Hu, Y. Pi, *Nano Lett.* 10 (2010) 2604.
- [23] K. Yao, D. Caruntu, Z. Zeng, J. Chen, C.J. O’Connor, W. Zhou, *J. Phys. Chem. C* 113 (2009) 14812.
- [24] F. Li, X. Badel, J. Linnros, J.B. Wiley, *J. Am. Chem. Soc.* 127 (2005) 3268.
- [25] F. Li, Y. Ding, P.X. Gao, X.Q. Xin, Z.L. Wang, *Angew. Chem. Int. Ed.* 43 (2004) 5238.
- [26] Y. Zhang, Q. Xiang, J. Xu, P. Xu, Q. Pana, F. Li, *J. Mater. Chem.* 19 (2009) 4701.
- [27] D.R. Kauffman, D.C. Sorescu, D.P. Schofield, B.L. Allen, K.D. Jordan, A. Star, *Nano Lett.* 10 (2010) 958.
- [28] Z. Jiang, J. Wang, L. Meng, Y. Huang, L. Liu, *Chem. Commun.* 47 (2011) 6350.
- [29] Y. Dan, Y. Lu, N.J. Kybert, Z. Luo, A.T.C. Johnson, *Nano Lett.* 9 (2009) 1472.
- [30] V. Milman, B. Winkler, J.A. White, C.J. Pickard, M.C. Payne, E.V. Akhmatkaya, R.H. Nobes, *J. Quantum Chem.* 77 (2000) 895.
- [31] Q. Zhao, M.B. Nardelli, W. Lu, J. Bernholc, *Nano Lett.* 5 (2005) 847.
- [32] Y. Zhang, D. Zhang, C. Liu, J. Phys. Chem. B 110 (2006) 4671.
- [33] F. Tournus, J.-C. Charlier, *Phys. Rev. B* 71 (2005) 165421.

- [34] J. Taylor, H. Guo, J. Wang, *Phys. Rev. B* 63 (2001) 245407.
- [35] W.L. Yim, X.G. Gong, Z.F. Liu, *J. Phys. Chem. B* 107 (2003) 9363.
- [36] P. Sjövall, S.K. So, B. Kasemo, R. Franchy, W. Ho, *Chem. Phys. Lett.* 172 (1990) 125.
- [37] J. Dai, J. Yuan, P. Giannozzi, *Appl. Phys. Lett.* 95 (2009) 232105.
- [38] Z. Zhou, X. Gao, J. Yan, D. Song, *Carbon* 44 (2006) 939.
- [39] Y. Zou, F. Li, Z.H. Zhu, M.W. Zhao, X.G. Xu, X.Y. Su, *Eur. Phys. J. B* 81 (2011) 475.
- [40] Y. Chen, B. Gao, J.-X. Zhao, Q.-H. Cai, H.-G. Fu, *J. Mol. Model.* 18 (2012) 2043.
- [41] L. Bai, Z. Zhou, *Carbon* 45 (2007) 2105.
- [42] S. Peng, K. Cho, *Nano Lett.* 3 (2003) 513.
- [43] L.B.D. Silva, S.B. Fagan, R. Mota, *Nano Lett.* 4 (2004) 65.
- [44] R. Chen, N. Franklin, J. Kong, J. Cao, T. Tomblor, Y. Zhang, H. Dai, *Appl. Phys. Lett.* 79 (2001) 2258.
- [45] M.P. Hyman, J.W. Medlin, *J. Phys. Chem. B* 109 (2005) 6304.
- [46] D.-H. Lim, A.S. Negreira, J. Wilcox, *J. Phys. Chem. C* 115 (2011) 8961.
- [47] E. König, S. Kremer, *Theoret. Chim. Acta (Berl.)* 23 (1971) 12.
- [48] G.L. Miessler, D.A. Tarr, *Inorganic Chemistry*, third ed., Pearson/Prentice Hall, 2004.
- [49] H.L. Schläfer, G. Gliemann, Wiley Interscience, New York, 1969.
- [50] H.S. Kang, *J. Am. Chem. Soc.* 127 (2005) 9839.